Diffraction at Rounded Wedges: MoM Modeling of PTD Fringe Waves

Gokhan Apaydin [1], Levent Sevgi [2], and Pyotr Ya Ufimtsev [3]

[1] Electromagnetic Consulting, Istanbul, Turkey
g.apaydin@gmail.com

[2] Department of Electrical-Electronics Engineering
Okan University, Tuzla, Istanbul, 34759, Turkey
levent.sevgi@okan.edu.tr

[3] EM Consulting, Los Angeles, California, 90025, USA
pufimtsev@gmail.com

Abstract ─ The paper examines diffraction at rounded wedges with perfectly conducting faces. This topic was a subject of many publications which investigated mainly the *total* diffracted waves. In the present paper, we calculate specifically their *fringe* components to illustrate their sensitivity to the edge curvature. Such fringe waves provide substantial contributions to the scattered field in certain directions and represent a key element in extension of the physical theory of diffraction (PTD) for objects with rounded edges.

Index Terms ─ Fringe wave, hard boundary condition, method of moments, non-uniform currents, physical optics, physical theory of diffraction, rounded wedge, soft boundary condition, uniform currents.

I. INTRODUCTION

A number of papers exist which studied diffraction at wedges with rounded edges. Perhaps the first one was the Kalashnikov paper [1] where he presented the first objective validation of the Sommerfeld diffraction theory. He accomplished thorough experimental investigation of light waves diffracted at metallic wedges with finite edge curvature. In publications [2-24], one can find additional references. Main subjects in those publications were the *total* waves scattered at the edges. Our objective is to calculate specifically their *fringe* components which are the most sensitive to the edge curvature. Such fringe waves provide substantial contributions to the scattered field away from the boundaries of incident and reflected waves. They represent a key element for extension of the physical theory of diffraction (PTD) to objects with rounded edges.

The paper is organized as follows. Section 2 describes the geometry of the problem. In Section 3, we formulate the integral equations in the PTD format for the fringe currents [5,6,25,26]. Section 4 presents their solution by method of moments (MoM) and illustrates fringe waves scattered at curved edges in comparison with those scattered at sharp wedges.

The time dependence $\exp(-i\omega t)$ is used in the paper.

II. GEOMETRY OF THE PROBLEM

A wedge with a rounded edge is constructed as a combination of the circular cylinder smoothly conjugated with the wedge faces (see, Fig. 1). The wedge with interior angle 2β is located symmetrically along x-axis on the two-dimensional (2D) xy-plane. The origin coincides with the apex of the sharp wedge. Here, a is the radius of the cylindrical surface L_0. Points (x_j,y_j) and $(x_j,-y_j)$ are the junctions/tangency points of the cylindrical surface L_0 with two half-planes L_1, and L_2, which are the faces of the tangential wedge. Fringe waves calculated below for rounded edges are compared with those for the tangential wedge with infinite sharpness (a=0). The wedge is illuminated (from the left) by a plane incident wave propagating along the x-axis. In other words, only double side fixed illumination is considered.

Electromagnetic (EM) waves with two basic polarizations may be investigated for this scenario: the waves with the electric vector (magnetic vector) parallel to the edge of the PEC wedge. In the acoustic diffraction problem, these two situations relate to the wedge with the *soft (hard)* boundary conditions (SBC and HBC), respectively. The solutions of these two-dimensional EM and acoustic problems are identical [5,6].

The wedge structure is canonical in terms of extracting/visualizing every wave phenomenon occurs there [16]. Electromagnetic and acoustic waves interact with objects and scatter. The word *scattering* includes *reflection*, *refraction*, and *diffraction*. The addition of the *scattered field* and the *incident field* yields *total fields*.

The 2D scattering plane around the wedge may be divided into three regions in terms of critical wave

Submitted On: November 15, 2016
Accepted On: February 14, 2017

1054-4887 © ACES

phenomena occurred there [16]. In the first region, all three field components (incident field, reflected field, and diffracted field) exist. In the second (reflection-free) region, only incident and diffracted fields exist. These two regions are separated by the *reflection shadow boundary*.

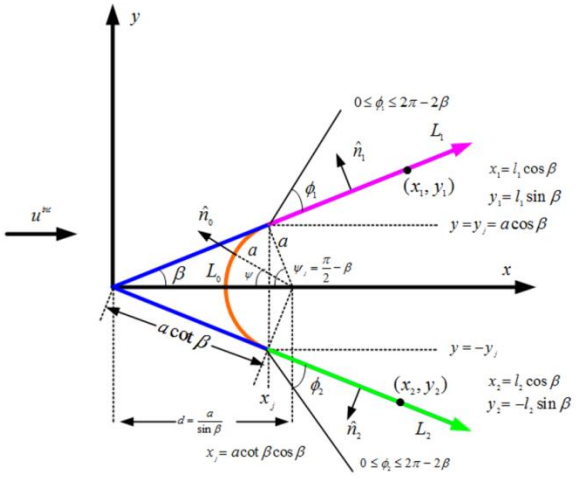

Fig. 1. Rounded wedge with perfectly reflecting faces.

For the sake of clear understanding and completeness, the definitions of total, scattered, diffracted, and fringe fields are included. *Total field* is the addition of the *incident* and *scattered fields*. In other words, in order to obtain scattered field, one needs to extract/subtract the incident field from the total field. The subtraction of the incident and reflected fields from the total field yields the diffracted field. In other words, the *diffracted field* is equal to the *scattered field* minus the *reflected field*. The f*ringe field* is the part of diffracted field generated by the source-induced fringe (*nonuniform*) currents. These currents exist because of any deviations of a scattering surface from a tangential plane [5,6]. Such deviations can be in the form of sharp discontinuities (edges, tips), discontinuity of a surface curvature (as in the junction points (x_j,y_j), $(x_j,-y_j)$) as well as the smooth bending (as in the cylindrical surface L_0).

As observed in Fig. 2, there are two points that can be taken as the origin. The first is the origin of the *xy*-coordinate system (*0,0*). For the computation of fields around the wedge for both sharp and rounded wedges the receivers are located on the observation circle with this origin and with a specified radius. In this case, the coordinates (r,φ) related to the sharp wedge are used. The second origin is the center of the rounded-part of the rounded wedge (*d,0*) where we use coordinates (ρ,ψ) related to the rounded wedge. In this case, fields around the rounded wedge are computed for the receivers located on the observation circle with this origin and with a specified radius. Figure 2 presents these two cases. Note that, reflections occur only in the shaded area for the sharp wedge but occur everywhere for the rounded wedge.

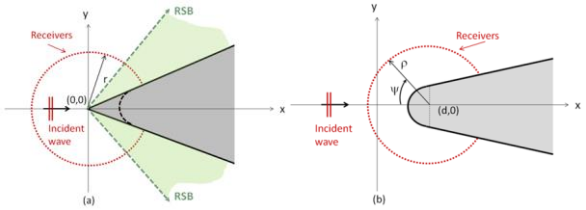

Fig. 2. Scenarios for: (a) sharp–rounded wedge comparisons, and (b) fields simulated around the rounded wedge.

III. FORMULATION OF INTEGRAL EQUATIONS

In the problem under investigation, we apply a scalar interpretation for a perfectly conducting wedge. The soft boundary condition u=0 relates to excitation of the wedge by the *E*-polarized plane wave:

$$u^{inc} = E_z^{inc} = u_0 e^{ikx}. \tag{1}$$

The hard boundary condition ($\partial u/\partial n = 0$) corresponds to the case when the wedge is illuminated by the *H*-polarized plane wave:

$$u^{inc} = H_z^{inc} = u_0 e^{ikx}. \tag{2}$$

Proceeding with the second Green's identity one can obtain the surface integral equation:

$$u^{inc}(x,y) + \frac{i}{4} p.v.\int_L \left[u(x',y') \frac{\partial}{\partial n} H_0^{(1)}(kr) - \frac{\partial u(x',y')}{\partial n} H_0^{(1)}(kr) \right] dl' = \frac{u(x,y)}{2}. \tag{3}$$

Here, L=L_0+L_1+L_2 is the total surface of the body, $r = \sqrt{(x-x')^2 + (y-y')^2}$, and the integrand is singular at the point r=0. The integral is understood as its Cauchy principal value. The incident wave u^{inc} in (3) is given everywhere on the surface L. Function u is the total field u=u^{inc}+u^{sc}. It follows from (3) that,

$$u^{inc}(x,y) - \frac{i}{4} p.v.\int_L \frac{\partial u_s(x',y')}{\partial n} H_0^{(1)}(kr) dl' = 0, \tag{4}$$

for the soft surface (u=0), and,

$$u^{inc}(x,y) + \frac{i}{4} p.v.\int_L u_h(x',y') \frac{\partial}{\partial n} H_0^{(1)}(kr) dl' = \frac{u(x,y)}{2}, \tag{5}$$

for the hard surface ($\partial u/\partial n = 0$).

Now, we recast these equations in the PTD format [5,6]. First, introduce the surface currents:

$$j_s = \frac{\partial u_s}{\partial n}, j_h = u_h. \tag{6}$$

They consist of two components:

$$j_{s,h} = j_{s,h}^{(0)} + j_{s,h}^{(1)} = j_{s,h}^{PO} + j_{s,h}^{fr}, \quad (7)$$

where $j^{(0)} = j^{PO}$ is the uniform component defined according to the physical optics (PO). It is defined as:

$$j_s^{PO}(x',y') = 2\frac{\partial u^{inc}}{\partial n}, \; j_h^{PO}(x',y') = 2u^{inc}. \quad (8)$$

The term $j_{s,h}^{fr}$ represents the non-uniform PTD component called here the fringe current. In view of these notations, Equations (4) and (5) take the forms:

$$\frac{i}{4} p.v.\int_L j_s^{fr}(x',y') H_0^{(1)}(kr) dl' = u^{inc}(x,y) - \frac{i}{4} p.v.\int_L j_s^{PO}(x',y') H_0^{(1)}(kr) dl', \quad (9)$$

$$\frac{1}{2} j_h^{fr}(x,y) - \frac{i}{4} p.v.\int_L j_h^{fr}(x',y') \frac{\partial}{\partial n} H_0^{(1)}(kr) dl' = \frac{i}{4} p.v.\int_L j_h^{PO}(x',y') \frac{\partial}{\partial n} H_0^{(1)}(kr) dl'. \quad (10)$$

Calculating $j_{s,h}^{fr}$ from (9) and (10), one can find the total fringe waves scattered by the object as:

$$u_s^{fr}(x,y) = -\frac{i}{4}\int_L j_s^{fr}(x',y') H_0^{(1)}(kr) dl', \quad (11)$$

$$u_h^{fr}(x,y) = \frac{i}{4}\int_L j_h^{fr}(x',y') \frac{\partial}{\partial n} H_0^{(1)}(kr) dl'. \quad (12)$$

As shown in [6,25], the integrals from $j_{s,h}^{PO}$ over the faces $L_{1,2}$ represent the PO fields scattered by half-planes. They are described in accordance with (3.37-3.40) and (3.49), (3.50) of [6]. The details of their calculations are presented in [25] that contain the fringe integral equations similar to (9), (10). The only difference in (9), (10) consists in presence of integrals over the cylindrical part L_0.

For numeric solution of the fringe integral Equations (9), (10) we apply the classical MoM (see, [14,20] for details).

IV. NUMERICAL SIMULATIONS AROUND SHARP AND ROUNDED WEDGES

The MoM related references mentioned above in the Introduction show that MoM is highly capable of solving surface integral equations. Here, we develop the MoM algorithms for the fringe integral equations derived in the previous section and first test them against the sharp wedge. Note that, in addition to the fringe fields, the total, scattered, and PO scattered field variations around the wedge are also given for clear understanding of wave scattering phenomena (see, [16,18] for detailed illustrations of diffracted fields). Fringe fields are directly computed using (11), (12). One needs to add PO scattered fields in order to obtain total scattered fields. Finally, addition of the incident field to the scattered field yields the total field.

Numerical simulations in this section consist of two parts. As shown in Fig. 2 (a), the first computations belong to various fields from the rounded wedge and their comparison with that from the sharp wedge. The frequency of all simulations is 30 MHz (i.e., λ=10 m). The observer radius is $r=2\lambda$. Although infinite, the length of L_1 and L_2 parts of the wedge is taken 50λ-long, which is tested to be enough for the accuracies used in these numerical calculations. Also, the number of segments in one wavelength is chosen as 20 for MoM calculations (in the vicinity of the edge up to 100-500 segments may be used to increase the accuracy). It is also numerically tested that the number of segments of the rounded part (L_0 part) is at least 20 to satisfy rounded curvature. Note that, different discretizations may be required for the wedges with soft and hard BCs [20]. Approximately, 10λ-20λ-long wedge sides are enough for the soft wedge but up to 100λ-long wedge sides (even more) may be required for the hard wedge.

In the second part, fields from the rounded wedge are computed for the scenario in Fig. 2 (b). It includes the fringe field, the PO field, and their sum.

For the soft sharp wedge, we denote $j_s^{fr}(x,y)$ as $j_s^{fr,shrp}(x,y)$ and outside the wedge it creates the field:

$$u_s^{fr,shrp}(x,y) = -\frac{i}{4}\int_L j_s^{fr,shrp}(x',y') H_0^{(1)}(kr) dl'. \quad (13)$$

This fringe field is calculated using (4.18) on p. 107 in [6]. This is assumed as the reference (PTD) solution. Alternatively, the MoM algorithm presented in [20,25] can be used directly. For the rounded wedge, (9) is discretized and solved using the new MoM algorithm and segment fringe currents $j_s^{fr,rnd}$ are obtained. Then, fringe fields $u_s^{fr,rnd}(x,y)$ around the object are calculated using (11).

In the following examples, for the sharp wedge, first the wedge (half) angle β=5°,15°,30°,45° is specified. Then, the observation circle with $r=2\lambda$ is chosen. On this circle, the receivers are located at grid points $x = r\cos(\beta+\varphi)$, $y = r\sin(\beta+\varphi)$ with $\Delta\varphi$=0.5°. Finally, because of the symmetry with respect to x axis, $\left|u_s^{fr,shrp}/u_0\right|$ for $0 \le \varphi \le \pi - \beta$ is calculated and plotted. For the rounded wedge, and for the same sets of parameters, $a=\lambda/m$, m=2,5,10,20,… is specified and MoM solutions are generated and $\left|u_s^{fr,rnd}/u_0\right|$ for $0 \le \varphi \le \pi - \beta$ is plotted. The objective is to demonstrate how $\left|u_s^{fr,rnd}/u_0\right|$ approaches $\left|u_s^{fr,shrp}/u_0\right|$ with decreasing of the rounding radius (a). Examples presented in Figs. 3-7 belong to SBC case; the next figures are given both for SBC and HBC cases.

Note that, the rounded wedge MoM model directly yields sharp wedge solutions when a=0. This is used in validating the new rounded wedge MoM algorithm. The rounded wedge algorithm is tested against both PTD and previous sharp MoM models and perfect agreement is obtained. Figure 3 belongs to these validations (a free MATLAB package has been prepared for the visualization of fringe waves around a sharp wedge and its tutorial has just been published [26]).

Figures 4-5 present total and fringe fields, respectively, with four different wedges for the scenario in Fig. 2 (a). The three curves belong to a=0, a=λ/10, and a=λ/5, cases. As observed in Fig. 4, major total field contribution comes from the interaction of incident, reflected, and diffracted waves. Total fields of the 90° wedge for all three cases are almost identical. The differences in the total fields around the wedge become significant as the wedge interior angle gets smaller. This is because the locations of the receivers shift significantly for narrow wedges (see, Fig. 2 (a)). The same observation also holds for the fringe field variations in Fig. 5.

For the sharp wedge only diffracted field occurs backwards (i.e., towards to the angle of incoming plane wave). But for the rounded wedge there is a strong backward reflection.

Note that, as a increases, the distance between the receiver on x-axis and backward specular reflection point increases and the amplitude of the scattered field along this direction decreases. The effect of this is observed in Fig. 5 where fringe field variation is plotted. However, for fringe waves another reason also exists for their decrease. The larger is radius a of rounded/cylindrical surface L_0 the smaller gets its curvature and, as a consequence, the smaller fringe currents become there.

PO and fringe fields around the rounded wedge are simulated in this section. The scenario for these simulations is given in Fig. 2 (b). For the calculation of this fringe field, first, β and a are chosen. Then, the receivers are located on the circle around the rounded wedge using the grid points (x,y) on the circle $\rho=a+n\lambda$, n=1,2,… with $0 \le \psi \le \psi_m$ and $\Delta\psi$=0.5° where,

$$\sin(\beta+\psi_m)=\frac{a}{\rho}. \qquad (14)$$

Then, (9) is discretized and solved using the new MoM algorithm and the segment fringe currents $j_s^{fr,rnd}$ are obtained. Fringe fields $u_s^{fr,rnd}(x,y)$ are then calculated using (11). Fringe fields vs. angle variations are then plotted.

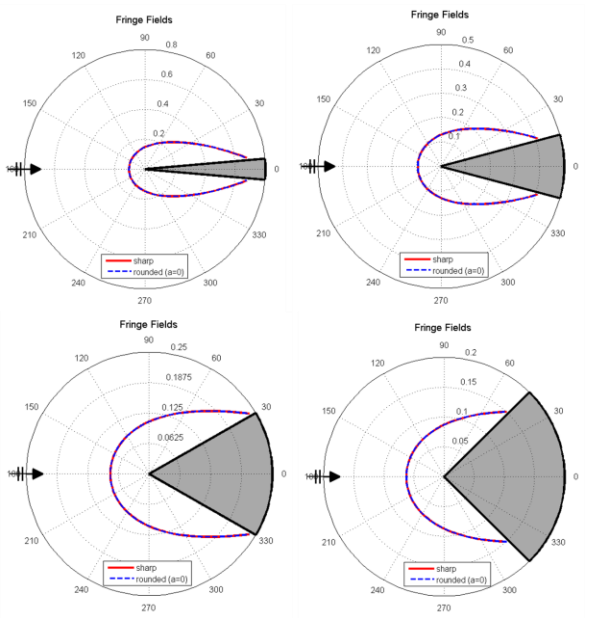

Fig. 3. Fringe fields around different SBC sharp wedges (for the scenario in Fig. 2 (a)). The solid (red) curve is calculated according to (4.18) in [6]. The dashed (blue) curve – by MoM.

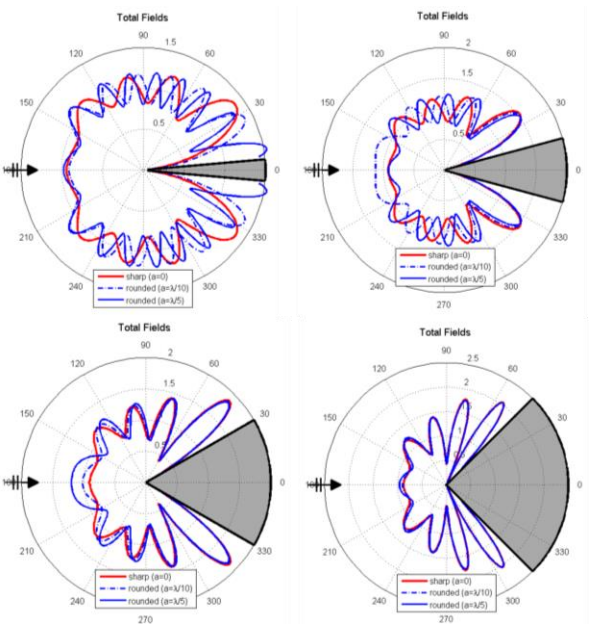

Fig. 4. Total fields around different SBC wedges (for the scenario in Fig. 2 (a)). The solid (red) curve is calculated according to (4.18) in [6]. Other curves – by MoM.

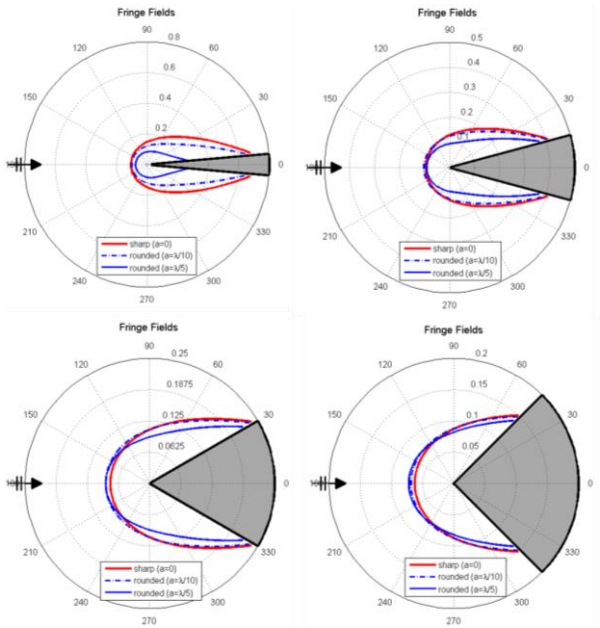

Fig. 5. Fringe fields around different SBC wedges (for the scenario in Fig. 2 (a)).

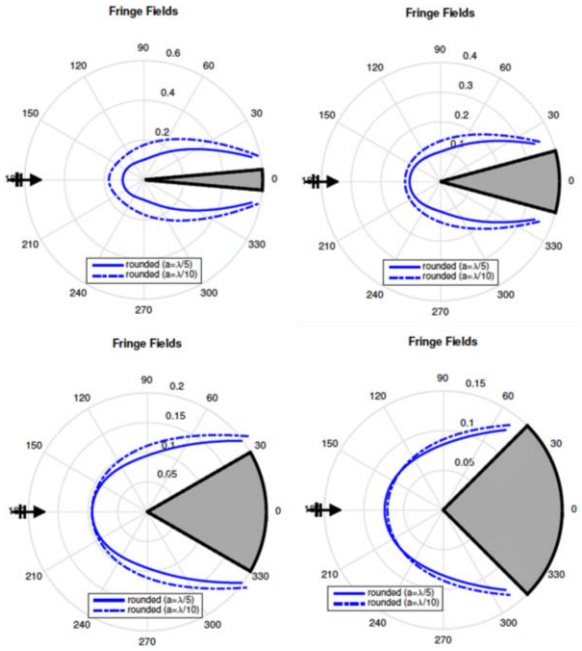

Fig. 6. Fringe fields around different SBC wedges (for the scenario in Fig. 2 (b)).

For the PO-scattered fields around the rounded wedge, we calculate the integral:

$$u_s^{PO,rnd}(x,y) = -\frac{i}{4}\int_L j_s^{PO}(x',y')H_0^{(1)}(kr)dl', \quad (15)$$

with $L = L_0 + L_1 + L_2$. Hence,

$$u_s^{PO,rnd}(x,y) = u_{s,L_0}^{PO,rnd} + u_{s,L_1}^{PO,rnd} + u_{s,L_2}^{PO,rnd}. \quad (16)$$

Here,

$$u_{s,L_0}^{PO,rnd}(x,y) = -u_0 e^{ikd}\frac{ka}{2} \times \int_{-\psi_j}^{\psi_j} \cos\psi\, e^{-ika\cos\psi} H_0^{(1)}(kr_0)d\psi, \quad (17)$$

with $r_0 = \sqrt{(x-x_0)^2+(y-y_0)^2}$,

$$u_{s,L_1}^{PO,rnd}(x,y) = u_0 e^{ikx_j} v_s^{(0)}(kr_1,\phi_1,\phi_0) + \begin{cases} -u_0 e^{ikx_j} e^{-ikr_1\cos(\phi_1+\phi_0)} & \text{for } 0 \le \phi_1 \le \beta \\ 0 & \text{for } \beta \le \phi_1 \end{cases}, \quad (18)$$

$$u_{s,L_2}^{PO,rnd}(x,y) = u_0 e^{ikx_j} v_s^{(0)}(kr_2,\phi_2,\phi_0), \quad (19)$$

for $\pi - \beta \le \phi_2 \le 2\pi - 2\beta$, where $\phi_{1,2}$ is found from (A.4). Also,

$$\begin{aligned} r_1 &= \sqrt{(x-x_j)^2+(y-y_j)^2} \\ r_2 &= \sqrt{(x-x_j)^2+(y+y_j)^2} \\ x_j &= d - a\cos\psi_j = d - a\sin\beta \\ y_j &= a\sin\psi_j = a\cos\beta \end{aligned}. \quad (20)$$

Notice that, $v_s^{(0)}(kr_1,\phi_1,\phi_0)$ is discontinuous on the boundary of the reflected plane wave ($\phi_1 = \beta$). In summary, $u_s^{PO,rnd}$ is calculated from (15) and (16) for the specified grid points and the results are plotted as PO fields vs. angle. The total field will then be the sum of these two:

$$u_s^{tot,rnd}(x,y) = u_s^{fr,rnd}(x,y) + u_s^{PO,rnd}(x,y). \quad (21)$$

Figure 6 belongs to the second scenario given in Fig. 2 (b) and shows fringe field distributions for four different wedge angles for two different a values ($a_1=\lambda/10$ and $a_2=\lambda/5$). Here, the receivers are located on a circle around the rounded wedge (not around the origin on the xy-plane) with the center at $(0,x_2)$ where $x_2 = d_2 = a_2/\sin\beta$ and radius $\rho_2=\lambda/5+2\lambda$. Although, the receivers for the computations for $a_1=\lambda/10$ and $a_2=\lambda/5$ are exactly at the same points, the difference of distances between the rounded face and the receivers for these two cases gets larger, for the receivers around the backscattering direction $\varphi=180°$.

Figure 7 shows uniform (PO), nonuniform (fringe), and total currents on the surface of the wedge having a 30° interior angle, and $a=\lambda/2$ for the SBC case. This figure clearly demonstrates that the fringe currents concentrate in vicinity of the junction points, i.e., in vicinity of the surface curvature discontinuities. Tests with different sets of parameters show that the strongest fringe currents occur for the sharp wedge ($a=0$). The fringe current decays on both sides of the junction points and has a minimum at midpoint between the junctions.

Figure 8 compares fringe currents of both SBC and HBC cases a few λ around junction points. Here, although L_1=L_2=50λ is used in the MoM computations, only L_1=L_2=4.35λ and L_0=1.3λ sections are shown in the figure (i.e., horizontal axis extends from -5λ to 5λ) with λ/40 discretization. Nearly, 500 segments are used for the rounded part L_0 (with a=λ/2, this corresponds to a nearly λ/400 segmentation). Very small segments are used just to increase the accuracy around the junctions.

As seen there, the fringe current distributions of SBC and HBC cases look alike; they have maxima on the junction points. However, SBC fringe currents make sharp peaks on the junction points but HBC fringe currents have slight discontinuities. Also, HBC fringe currents are higher than SBC fringe currents. Finally, both fringe currents decay away from junctions but HBC fringe currents' decay rate is lower than SBC fringe currents.

Here, it is pertinent to remind the fringe currents behavior in vicinity of a sharp wedge. In SBC case, the fringe current tends to infinity as $(1/kr)^{1-\pi/\alpha} \to \infty$, while in HBC case it is finite ($j_h^{fr} = u_0(4\beta - 2\pi)/\alpha$) when $r \to 0$ and $\alpha = 2\pi - 2\beta > \pi$ [6,27]. Because j_h^{fr} is finite for sharp wedges it is not surprising that it has only slight changes in vicinity of the junction points where the surface L is smooth and only its second derivative undergoes discontinuities.

Remind also that, away from the edge ($kr >> 1$) on the sharp wedge (with β=15°) the SBC current j_s^{fr} drops as $(1/kr)^{3/2}$ while the HBC current j_h^{fr} attenuates as $(1/kr)^{1/2}$ [6]. The curves in Fig. 8 for $|r| > 3\lambda$ relate to large values ($kr > 18$) and qualitatively agree with those for a sharp wedge. Notice as well that at point ψ=0 (r=0 in Fig. 8) on the circular cylinder alone (without L_1, L_2), the SBC and HBC fringe currents are determined by (14.53) and (14.54) of [6] where one should set $\gamma = \pi/2$ and $\psi = -\pi/2$. According to these equations, $\left|j_s^{fr}\right| = k\left|j_h^{fr}\right|$. For λ=10m (with f=30 MHz) taken in our calculations this relationship means that $\left|j_s^{fr}\right| \approx 0.6\left|j_h^{fr}\right|$, while for the rounded wedge according to Fig. 8 we have $\left|j_s^{fr}\right| \approx 0.7\left|j_h^{fr}\right|$.

Finally, in Fig. 9 for comparison purpose we plot both the soft and hard fringe waves for rounded wedges with a=a_2=λ/5 at the distance ρ=a_2+2λ. They relate to the scenario in Fig. 2 (b). Notice that, the curves for the wedge with β=30° are similar to those for the sharp wedge given in Fig. A4.5 of [6].

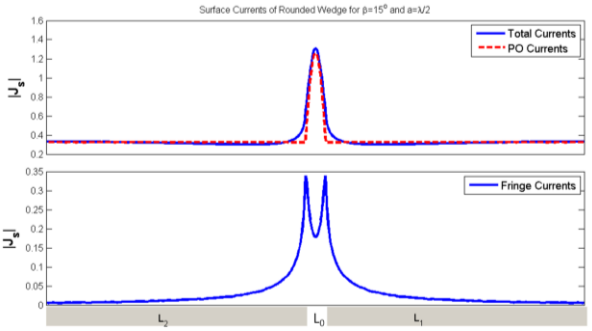

Fig. 7. Total, PO and PTD (fringe) surface currents of the 30° SBC wedge.

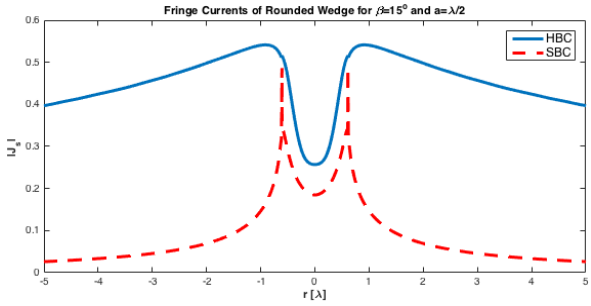

Fig. 8. PTD (fringe) surface currents of the 30° SBC and HBC wedges.

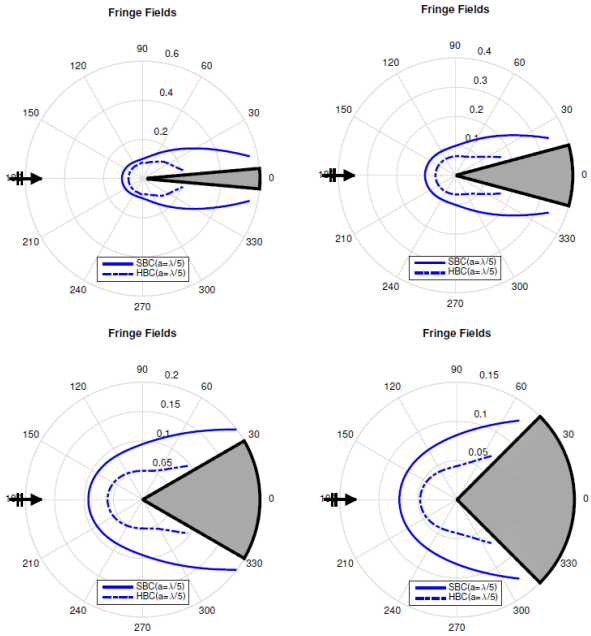

Fig. 9. Fringe fields around different SBC/HBC wedges (for the scenario in Fig. 2 (b)).

V. CONCLUSIONS

Fringe integral equations suitable for analysis of the field scattered by rounded soft and hard wedges are developed. Numeric results are obtained via a regular MoM procedure. Comparison with scattering from sharp wedges is illustrated and confirms that the rounded wedge can be considered, approximately, as the sharp wedge when the radius of rounding does not exceed one tenth of the wavelength. The results are also important from the theoretical/methodical point of view because they demonstrate the direct extension of PTD for objects with rounded edges.

REFERENCES

[1] A. Kalashnikov, "The Gouy-Sommerfeld diffract-tion," (in Russian) *J. Russian Physical-Chem. Soc*., vol. 44, Physical Section, St. Petersburg, Russia, no. 3, pp. 137-144, 1912.

[2] C. Hansen, Ed., *Geometrical Theory of Diffraction*. IEEE Press, 1981.

[3] J. J. Bowman, T. B. A. Senior, and P. L. E. Uslenghi, Eds., *Electromagnetic and Acoustic Scattering by Simple Shapes.* Hemisphere Publishing Corporation, 1987.

[4] Y. A. Kravtsov and N. Y. Zhu, *Theory of Diffraction: Heuristic Approaches*. Alpha Science Series on Wave Phenomena, 2010.

[5] P. Y. Ufimtsev, *Fundamentals of the Physical Theory of Diffraction.* John Wiley & Sons, Inc., Hoboken, New Jersey, USA, 2007.

[6] P. Y. Ufimtsev, *Fundamentals of the Physical Theory of Diffraction*. Second Edition, John Wiley & Sons, Inc., Hoboken, New Jersey, USA, 2014.

[7] M. A. K. Hamid, "Diffraction coefficient of a conducting wedge loaded with a cylindrical dielectric slab at the apex," *IEEE Trans. Antennas Propagat*., vol. AP-21, pp. 398-399, May 1973.

[8] A. Elsherbeni and M. Hamid, "Diffraction by a wide double wedge with rounded edges," *IEEE Trans. Antennas Propagat*., vol. AP-33, pp. 1012-1015, Sep. 1985.

[9] W. Hallidy, "On uniform asymptotic Green's function for the perfectly conducting cylinder tipped wedge," *IEEE Trans. Antennas Propagat*., vol. AP-33, no. 9, pp. 1020-1025, Sep. 1985.

[10] K. M. Mitzner, K. J. Kaplin, and J. F. Cashen, "How scattering increases as an edge is blunted," In the book: H. N. Kriticos and D. L. Jaggard (Editors), *Recent Advances in Electromagnetic Theory*. Springer, 1990.

[11] E. N. Vasiliev, V. V. Solodukhov, and A. I. Fedorenko, "The integral equation method in the problem of electromagnetic waves diffraction by complex bodies," *Electromagnetics*, vol. 11, no. 2, pp. 161-182, Oct. 2007.

[12] I. G. Yarmakhov, "Investigation of diffraction of electromagnetic waves at edges of perfectly conducting and impedance wedges with a rounded edge," (in Russian - *Radiotekhnika I Elektronika*, vol. 36, no. 10, pp. 1887-1895, 1991) *J. Commun. Technol. Electron*., vol. 49, no. 4, pp. 379, 2004.

[13] M. A. Christou, A. C. Polycarpou, and N. C. Papanicolau, "Soft polarization diffraction coefficient for a conducting cylinder-tipped wedge," *IEEE Trans. Antennas Propagat*., vol. AP-58, no. 12, pp. 4082-4085, Dec. 2010.

[14] C. A. Balanis, L. Sevgi, and P. Y. Ufimtsev, "Fifty years of high frequency diffraction," *Int. Journal RF Microwave Computer-Aided Eng.*, vol. 23, no 4, pp. 394-402, July 2013.

[15] P. Y. Ufimtsev, "The 50-year anniversary of the PTD: Comments on the PTD's origination and development," *IEEE Antennas Propagat. Mag*., vol. 55, no. 3, pp. 18-28, June 2013.

[16] F. Hacivelioglu, L. Sevgi, and P. Y. Ufimtsev, "Electromagnetic wave scattering from a wedge with perfectly reflecting boundaries: Analysis of asymptotic techniques," *IEEE Antennas Propagat. Mag.*, vol. 53, pp. 232-253, June 2011.

[17] G. Cakir, L. Sevgi, and P. Y. Ufimtsev, "FDTD modeling of electromagnetic wave scattering from a wedge with perfectly reflecting boundaries: Comparisons against analytical models and calibration," *IEEE Trans. Antennas Propagat.*, vol. AP-60, no. 7, pp. 3336-3342, July 2012.

[18] F. Hacivelioglu, M. A. Uslu, and L. Sevgi, "A Matlab-based simulator for the electromagnetic wave scattering from a wedge with perfectly reflecting boundaries," *IEEE Antennas Propagat. Mag*., vol. 53, no. 6, pp. 234-243, Dec. 2011.

[19] M. A. Uslu and L. Sevgi, "Matlab-based virtual wedge scattering tool for the comparison of high frequency asymptotics and fdtd method," *Appl. Comput. Electromagn. Soc. J.*, vol. 27, no. 9, pp. 697-705, Sep. 2012.

[20] G. Apaydin and L. Sevgi, "A novel wedge diffraction modeling using method of moments (mom)," *Appl. Comput. Electromagn. Soc. J.*, vol. 30, no. 10, pp. 1053-1058, Oct. 2015.

[21] M. A. Uslu, G. Apaydin, and L. Sevgi, "Double tip diffraction modeling: finite difference time domain vs. method of moments," *IEEE Trans. Antennas Propagat.*, vol. AP-62, no. 12, pp. 6337-6343, Dec. 2014.

[22] F. Hacivelioglu, L. Sevgi, and P. Y. Ufimtsev, "Wedge diffracted waves excited by a line source: exact and asymptotic forms of fringe waves," *IEEE Trans. Antennas Propagat*., vol. AP-61, no. 9, pp. 4705-4712, Sep. 2013.

[23] A. K. Bhattacharyya, "Scattering by a right-angled penetrable wedge: A stable hybrid solution (tm case)," *Appl. Comput. Electromagn. Soc. J.*, vol. 5,

no. 3, 1990.

[24] T. Ikiz and M. K. Zateroglu, "Diffraction of obliquely incident plane waves by an impedance wedge with surface impedances being equal to the intrinsic impedance of the medium," *Appl. Comput. Electromagn. Soc. J.*, vol. 26, no. 3, pp. 199-205, Mar. 2011.

[25] G. Apaydin, L. Sevgi, and P. Y. Ufimtsev, "Fringe integral equations for the 2-D wedge with soft and hard boundaries," *Radio Science*, vol. 61, no. 9, pp. 4705-4712, Sep. 2016.

[26] G. Apaydin and L. Sevgi, "Two dimensional non-penetrable wedge scattering problem and a Matlab-based fringe wave calculator," *IEEE Antennas Propagat. Mag.*, vol. 58, no. 2, pp. 86-93, Apr. 2016.

[27] P. Y. Ufimtsev, "Fast convergent integrals for nonuniform currents on wedge faces," *Electromagnetics*, vol. 18, no. 3, pp. 289-313, May-June 1998. Corrections in *Electromagnetics*, vol. 19, no. 5, pp. 473, 1999.

Gökhan Apaydin received the Ph.D. degree from Bogazici University, Istanbul in 2007. He was with Bogazici University from 2001 to 2005; the University of Technology Zurich from 2005 to 2010; Zirve University, Gaziantep from 2010 to 2016; and he was a Visiting Associate Professor at the Department of ECE, University of Illinois at Urbana–Champaign, IL, USA, in 2015. He has been involved with complex electromagnetic problems and systems. His research interests include analytical and numerical methods (FEM, MoM, FDTD) in electromagnetics (especially on electromagnetic computation of wave propagation, diffraction modeling, and related areas).

Levent Sevgi received the Ph.D. degree from Istanbul Technical University (ITU), and Polytechnic Institute of New York University, Brooklyn, in 1990. Prof. Leo Felsen was his Advisor. He was with ITU (1991-1998); the Scientific and Technological Council of Turkey–Marmara Research Institute, Gebze/Kocaeli (1999-2000); Weber Research Institute/Polytechnic University in New York (1988-1990); the Scientific Research Group of Raytheon Systems, Canada (1998-1999); the Center for Defense Studies, ITUVSAM (1993-1998) and (2000-2002); the Department of ECE, UMASS Lowell, MA (2012-2013) for his sabbatical term; and Doğuş University (2001-2014). Since 2014, he has been with Okan University, Istanbul. He has been involved with complex electromagnetic problems and systems for ~ 30 years.

Pyotr Ya. Ufimtsev received the Ph.D. degree in Radio Engineering from the Central Research Radio Engineering Institute of the Defense Ministry, Moscow in 1959, and the Dr.Sc. degree in Theoretical and Mathematical Physics from St. Petersburg University in 1970. He was with the Institute of Radio Engineering and Electronics of the Academy of Sciences, Moscow; the Moscow Aviation Institute; Northrop-Grumman Corp., CA; the University of California at Los Angeles, and the University of California at Irvine. Among his fundamental results are the theory of scattering from black objects, the physical theory of diffraction, and the discovery of new physical phenomena related to surface waves in absorbing materials.